



Title	Coordinated Upper-Troposphere-to-Stratosphere Balloon Experiment in Biak
Author(s)	Hasebe, F.; Aoki, S.; Morimoto, S.; Inai, Y.; Nakazawa, T.; Sugawara, S.; Ikeda, C.; Honda, H.; Yamazaki, H.; Halimurrahman; Komala, N.; Putri, F. A.; Budiyo, A.; Soedjarwo, M.; Ishidoya, S.; Toyoda, S.; Shibata, T.; Hayashi, M.; Eguchi, N.; Nishi, N.; Fujiwara, M.; Ogino, S.-Y.; Shiotani, M.; Sugidachi, T.
Citation	Bulletin of the American Meteorological Society, 99(6), 1213-1230 https://doi.org/10.1175/BAMS-D-16-0289.1
Issue Date	2018-06-27
Doc URL	http://hdl.handle.net/2115/72228
Rights	© Copyright 2018.6.27 American Meteorological Society (AMS). Permission to use figures, tables, and brief excerpts from this work in scientific and educational works is hereby granted provided that the source is acknowledged. Any use of material in this work that is determined to be "fair use" under Section 107 of the U.S. Copyright Act or that satisfies the conditions specified in Section 108 of the U.S. Copyright Act (17 USC § 108) does not require the AMS' s permission. Republication, systematic reproduction, posting in electronic form, such as on a website or in a searchable database, or other uses of this material, except as exempted by the above statement, requires written permission or a license from the AMS. All AMS journals and monograph publications are registered with the Copyright Clearance Center (http://www.copyright.com). Questions about permission to use materials for which AMS holds the copyright can also be directed to permissions@ametsoc.org . Additional details are provided in the AMS Copyright Policy statement, available on the AMS website (http://www.ametsoc.org/CopyrightInformation).
Type	article
File Information	bams-d-16-0289.1.pdf



[Instructions for use](#)

COORDINATED UPPER-TROPOSPHERE-TO-STRATOSPHERE BALLOON EXPERIMENT IN BIAK

F. HASEBE, S. AOKI, S. MORIMOTO, Y. INAI, T. NAKAZAWA, S. SUGAWARA, C. IKEDA, H. HONDA, H. YAMAZAKI, HALIMURRAHMAN, N. KOMALA, F. A. PUTRI, A. BUDIYONO, M. SOEDJARWO, S. ISHIDOYA, S. TOYODA, T. SHIBATA, M. HAYASHI, N. EGUCHI, N. NISHI, M. FUJIWARA, S.-Y. OGINO, M. SHIOTANI, AND T. SUGIDACHI

This article introduces CUBE, a big-balloon air sampling field study conducted in Indonesia, and describes the scientific scope from a historical perspective through challenges in the coordination of the campaign.

Stratospheric change is a subject of unresolved scientific inquiry relevant to global climate. For example, the long-term trend of stratospheric turnover time is a matter of debate. In this article, we introduce the Coordinated Upper-Troposphere-to-Stratosphere Balloon Experiment in Biak (CUBE/Biak). Conducted in Indonesia, this experiment is a collaborative endeavor of the Cryogenic Air Sampling (CAS) group, the Soundings of Ozone and Water in the Equatorial Region (SOWER) group, and the National Institute of Aeronautics and Space of the Republic of Indonesia (LAPAN) in an effort to answer such questions (Fig. 1).

WHY DO WE NEED CUBE/BIAK? The atmospheric water content falls sharply toward the upper troposphere in response to the decrease of temperature and the associated drop in saturation water vapor pressure (Clausius–Clapeyron equation) with respect to height. As the air entering the stratosphere must cross the cold tropopause, the stratosphere is extremely dry; water molecules constitute only ≈ 4 parts per million (ppm). As a strong greenhouse gas, however, stratospheric water vapor could drive decadal-scale perturbations in global temperature (Solomon et al. 2010).

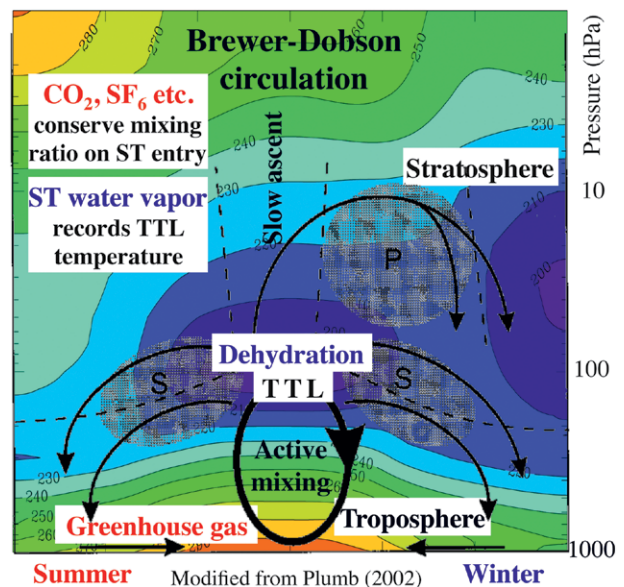


FIG. 1. Scope of CUBE/Biak illustrating the residual mean meridional circulation (curved arrows) driven by the breaking of synoptic (S) waves and planetary (P) waves (shaded regions), and the tropospheric Hadley circulation (heavy ellipse) taken from Plumb (2002). The background (color) is a schematic of the temperature distribution.

Where are we? The first description of the stratospheric general circulation was given by Brewer (1949), who noted that the midlatitude tropopause was not cold enough to explain stratospheric dryness. This notion, along with the interpretation of the global distribution of stratospheric ozone (Dobson 1956), crystallized into the classical view of stratospheric general circulation—the Brewer–Dobson circulation (BDC). Tropospheric air enters the stratosphere primarily through the cold tropical tropopause and spreads toward high latitudes in both hemispheres (the stratospheric portion of the arrows in Fig. 1).

Further investigation of radiosonde temperature data led to a hypothesis, the “stratospheric fountain” (Newell and Gould-Stewart 1981), in which the entry of air into the stratosphere was restricted, so as to be consistent with stratospheric dryness, to the western tropical Pacific in boreal winter and to the India–Bay of Bengal region in boreal summer. This hypothesis was accepted for a long time until Sherwood (2000) demonstrated that the lower-stratospheric vertical motion over the fountain was downward. How then could the tropospheric air enter the stratosphere?

The transformed Eulerian mean (TEM), a framework in which zonal mean circulation is driven by dissipation of planetary waves (Andrews and McIntyre 1976), helped answer this question. In the TEM formalism, the BDC is interpreted in terms of the “downward control principle” (Haynes et al. 1991) and “extratropical pump” (Holton et al. 1995) hypotheses that attribute the upward motion in the tropical stratosphere not to forcing by tropical convection but to a “suction pump” driven by dissipating planetary waves in the midlatitude stratosphere (occurring in the shaded region marked P in Fig. 1). Under these hypotheses, the tropospheric air could be pumped up

into the stratosphere irrespective of the downward motion over the stratospheric fountain.

The mystery of the peculiar downward motion was resolved with the concept of the tropical tropopause layer (TTL), a transition layer between the upper troposphere and the lower stratosphere. The TTL was introduced to recognize that the transition from the troposphere to the stratosphere takes place gradually in a layer rather than at a sharp boundary such as the tropopause (Atticks and Robinson 1983; Highwood and Hoskins 1998). It is located well above the main convective outflow but below the region in which extratropical pumping is effective (Fueglistaler et al. 2009). The tropospheric air lifted up by deep convection does not go directly into the stratosphere, except on rare occasions, as a result of the loss of buoyancy at around 10–15 km, but stays in the TTL subject to quasi-adiabatic horizontal motion. The downward motion over the stratospheric fountain merely means that the isentropes on which the air is constrained descend toward the wind direction.

The introduction of the TTL prompted another paradigm shift concerning the mechanism of water removal from the air entering the stratosphere. Since the earliest ideas of Brewer (1949), the low temperature of this air was attributed to the loss of internal energy of the air associated with an expansion along its ascent in convective clouds. This implication was overturned by the “cold trap” hypothesis (Holton and Gettelman 2001); it was exposure to low temperatures during horizontal advection that controlled the stratospheric water. This means the air must ascend adiabatically on its excursion in the TTL. This is made possible where the extension of cold region is maintained by a tropical thermally forced wind pattern, the so-called Matsuno–Gill pattern (Matsuno 1966; Gill 1980).

AFFILIATIONS: HASEBE—Faculty of Environmental Earth Science, Hokkaido University, Sapporo, Japan; AOKI, MORIMOTO, INAI, AND NAKAZAWA—Graduate School of Science, Tohoku University, Sendai, Japan; SUGAWARA—Faculty of Education, Miyagi University of Education, Sendai, Japan; IKEDA, HONDA, AND YAMAZAKI*—Institute of Space and Astronautical Science, Japan Aerospace Exploration Agency, Sagami, Japan; HALIMURRAHMAN, KOMALA, PUTRI, AND BUDIYONO—Atmospheric Science and Technology Center, LAPAN, Bandung, Indonesia; SOEDJARWO*—Biak Observatory, LAPAN, Biak, Indonesia; ISHIDOYA—National Institute of Advanced Industrial Science and Technology, Tsukuba, Japan; TOYODA—School of Materials and Chemical Technology, Tokyo Institute of Technology, Yokohama, Japan; SHIBATA—Graduate School of Environmental Studies, Nagoya University, Nagoya, Japan; HAYASHI, EGUCHI, AND NISHI—Faculty of Science, Fukuoka University, Fukuoka, Japan; FUJIWARA—Faculty of Environmental Earth Science, Hokkaido

University, Sapporo, Japan; OGINO—Japan Agency for Marine–Earth Science and Technology, Yokosuka, Japan; SHIOTANI—Research Institute for Sustainable Humanosphere, Kyoto University, Uji, Japan; SUGIDACHI—Meisei Electric Company, Ltd., Ise, Japan
*** CURRENT AFFILIATIONS:** YAMAZAKI—Space Industry Office, Ministry of Economy, Trade and Industries, Tokyo, Japan; SOEDJARWO—Satellite Technology Center, LAPAN, Bogor, Indonesia
CORRESPONDING AUTHOR: F. Hasebe, f-hasebe@ees.hokudai.ac.jp

The abstract for this article can be found in this issue, following the table of contents.

DOI:10.1175/BAMS-D-16-0289.1

In final form 27 December 2017

©2018 American Meteorological Society

For information regarding reuse of this content and general copyright information, consult the [AMS Copyright Policy](#).

This is an atmospheric response to equatorial thermal forcing from the surface and thus is most notable over the warm pool in the tropical western Pacific. See the discussion of “Background meteorological conditions” below for its detailed structure. This structure also plays a significant role in linking oceanic biological processes to stratospheric ozone chemistry. Depending on the residence time relative to the chemical lifetime in the TTL, the functionality of precursors of ozone depleting substances (ODSs) could be substantially different from that in the case of direct stratospheric injection [e.g., section 1.3 in WMO (2014)]. The dynamics and chemistry covering the whole altitude range from the boundary layer to the TTL were studied by coordinated aircraft campaigns: the Airborne Tropical Tropopause Experiment (Jensen et al. 2017), the Convective Transport of Active Species in the Tropics experiment (Pan et al. 2017), and the Coordinated Airborne Studies in the Tropics field campaign (Harris et al. 2017).

What is the step forward? The response of this basic tracer-coupled BDC to natural and anthropogenic forcing is one of the central issues of current stratospheric research (e.g., Waugh 2009). The increased concentration of greenhouse gases (GHGs) will enhance the wave transport of heat and momentum in the troposphere. The enhanced waves, propagating into the stratosphere, will modulate the BDC through the extratropical pump. Perturbations to the stratospheric turnover time will change the efficiency of the stratospheric removal of ODSs, which may necessitate a modification to predictions of future stratospheric ozone recovery.

Acceleration or deceleration of the BDC can be diagnosed by the decrease or increase of the age of air (AoA), the time elapsed since stratospheric air made its final contact with the troposphere (Kida 1983). We trace air parcels following atmospheric motion within the Lagrangian framework. The difficulty lies in the fact that, due to eddy mixing, any stratospheric air parcel is composed of various infinitesimal elements that have followed different pathways since stratospheric entry (Kida 1983; Hall and Plumb 1994; Waugh and Hall 2002). The distribution of transit times of all infinitesimal elements that constitute an air parcel is the age spectrum. It is not observable.

The mean value of stratospheric AoA, simply “mean age” hereafter, can be estimated by successive observations of “clock tracers” (Park et al. 2007; Ploeger et al. 2015) such as sulfur hexafluoride (SF_6) and carbon dioxide (CO_2). A clock tracer is chemically stable with a monotonically increasing mixing

ratio that acts as a traceable signal in the well-mixed troposphere. In the stratosphere, the mixing ratio is conserved following the atmospheric motion, keeping its value and thus memorizing the time of the last contact with the troposphere. The time lag between the increases of stratospheric and tropospheric air then gives an estimate of the mean age (Waugh and Hall 2002).

Analyzing 30 years of clock tracer data, Engel et al. (2009) found a small increase of 0.24 ± 0.22 yr decade⁻¹ in the mean age above 24 km in northern midlatitudes. This was statistically significant at the 68% confidence level but insignificant at the 90% level. This finding contradicts the long-term decrease of mean age diagnosed from simulations of chemistry–climate models that incorporated climate forcing such as changes of GHG, ODSs, aerosol amounts, and sea surface temperatures (e.g., Austin et al. 2007; Garcia and Randel 2008; McLandress and Shepherd 2009; Oman et al. 2009). This contradiction is not fully resolved in spite of intensive research efforts (e.g., Garcia et al. 2011; Stiller et al. 2012; Diallo et al. 2012).

An important piece missing in the analysis of Engel et al. (2009) was observational data in the tropical stratosphere. As compared to the mid- and high latitudes, the mean age must be younger, the effect of eddy mixing will be smaller, and thus, the age spectrum will have a more compact shape for an air parcel inside the “tropical pipe” (Plumb 1996) of mean ascent as a result of the protection by the subtropical mixing barrier. Observations in the tropics may help us examine the importance of lateral and vertical mixing that complicates the interpretation of mean age.

The focus on the tropics has additional advantages. One is the availability of what Mote et al. (1996) called the water vapor “tape recorder”: water anomalies gently ascending in the tropical stratosphere imprinted as stripes by seasonally varying tropopause temperature. This process is independent of clock tracers. Another quantity is gravitational separation; it becomes apparent in the atmosphere above the turbopause where molecular diffusion dominates over eddy mixing. Its detection in the stratosphere (Ishidoya et al. 2008, 2013) has given us another tool to investigate stratospheric circulation. Because of its one-dimensional nature due to gravity (Banks and Kockarts 1973a,b), it is less sensitive to horizontal mixing than to vertical advection and mixing and, thus, provides another independent measure of stratospheric transit time. The problem is how to realize stratospheric air sampling in the deep tropics, especially above the reach of aircraft.

CHALLENGES OF CUBE/BIAK. Whole air sampling with the aid of balloonborne cryogenic samplers is presently the most reliable method for studying the clock tracer distribution and gravitational separation in the stratosphere. The CAS group started air sampling over Japan in 1985 (Nakazawa et al. 1995), and extended it to the Arctic and Antarctic regions (Nakazawa et al. 2002; Aoki et al. 2003). The data analyzed by the CAS group constituted an important source of the age trend analysis by Engel et al. (2009). Collected samples have been used to analyze gravitational separation (Ishidoya et al. 2008) and fractionation of nitrous oxide (N_2O) isotopocules¹ (Toyoda et al. 2001) as well.

The SOWER group has been conducting field observations across the tropical Pacific to study TTL and stratospheric processes since 1998 (Fujiwara et al. 2001; Shiotani et al. 2002; Takashima et al. 2008). Ozonesondes and water vapor sondes have been launched together with conventional radiosondes.

¹ Isotopocules, formerly called isotopomers, are molecular species that only differ in either the number or position of isotopic substitutions. For example, $^{14}N^{15}N^{16}O$, $^{15}N^{14}N^{16}O$, and $^{14}N^{14}N^{18}O$ are isotopocules of N_2O . The abundance of each isotopocule is used to investigate photochemical decomposition and mixing of aged air masses in the stratosphere.

The combination of ozone and water is ideal for studying TTL transport because their strong vertical gradients, mostly positive in ozone (stratospheric source) while negative in water (tropospheric origin), make their mixing ratio sensitive to vertical motion. Simultaneous observations of aerosols by a Mie lidar provide important information on ice nucleation in TTL clouds (Shibata et al. 2007). In response to the proposal of the cold-trap hypothesis, SOWER focused on observations in the western tropical Pacific to investigate the efficiency of TTL dehydration (Fujiwara et al. 2010; Shibata et al. 2012; Hasebe et al. 2013; Inai et al. 2013) in collaboration with LAPAN.

LAPAN is the Indonesian space agency, founded in 1963. Along with space programs, it conducts atmospheric research (e.g., Trismidianto et al. 2016; Noersomadi and Tsuda 2017) by maintaining 10 ground-based stations and research facilities throughout Indonesia. They include meteor wind radar (Tsuda et al. 1995), wind profilers (Schafer et al. 2003), an X-band radar (Oigawa et al. 2017), and the Equatorial Atmosphere Radar. In 1992, LAPAN conducted a big-balloon launch, similar to that for cryogenic air sampling, and began successive ozonesonde observations at the Watukosek Observatory in Java (Komala et al. 1996). The Watukosek Observatory now constitutes part of the Southern Hemisphere

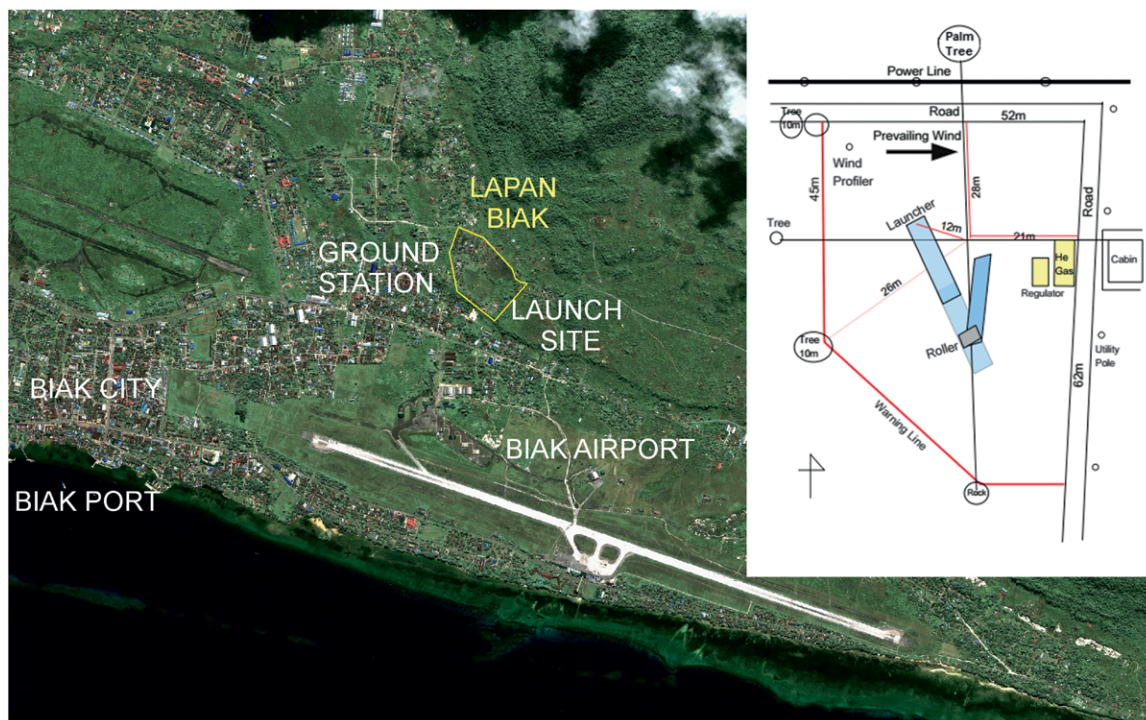


FIG. 2. Location of Biak station. Inset shows a sketch of the launch field. Blue rectangles denote the groundsheets used to protect the balloon material.

Additional Ozonesondes network (Thompson et al. 2003).

From these experiences emerged the idea of attempting a synthesized CAS–SOWER campaign in Indonesia in collaboration with LAPAN in January 2013. Considering the meteorological conditions, operational safety, and experiences accumulated by SOWER’s campaigns, LAPAN’s Biak station (1°10’S, 136°06’E) was chosen as the site of operations (Fig. 2). However, it was not until November 2014 that a technical agreement, a formal framework for conducting the campaign, was exchanged between the Japan Aerospace Exploration Agency (JAXA) and LAPAN—only 3 months before the scheduled campaign. Legal procedures (details in the appendix on “Additional information on legal issues”) were urgently followed including application for a foreign research permit (FRP) from the Ministry of Research and Technology (RISTEK)² of Indonesia, which was required to obtain a research visa; permissions for unmanned heavy (>6 kg) balloon launches to clear the rules of the International Civil Aviation Organization (ICAO); and security clearance from the Regional Directorate of Defense for vehicle and flight routes. The campaign was monitored by a security officer dispatched from the Ministry of Defense, Jakarta.

Cryogenic air-sampling instruments were shipped from Japan via Jakarta. One hundred helium gas cylinders were shipped from Singapore and three liquid nitrogen (LN) containers filled at Jakarta were combined with the instruments from Japan at Jakarta and transported to Biak. Transportation from Jakarta to Biak was undertaken by passenger vessel to shorten the travel time and minimize the loss of volatile LN. However, one of the three LN containers was found to be empty upon arrival at Biak, and an additional LN container (150 L) had to be transported urgently from Jakarta during the campaign. Pyro devices were transported by air in United Nations (U.N.) specification packaging because they were denied passage via ship. Express mail services were also used to send

² RISTEK has been restructured as the Ministry of Research, Technology, and Higher Education (Ristekdikti) at the time of writing.

TABLE 1. Launch sequence of instruments during CUBE/Biak; RS denotes radiosonde (instrument 1 in Table 2) and RS* was flown as a rehearsal for the recovery operation. Payload 1 comprises instruments 1, 2, 3, and 5; payload 2 consists of 1 and 4; payload 3 of 1 and 6; and payload 4 of 1 and 7. JTBK-A, -B, -C, and -D refer to the four cryogenic air samplers (instrument 8 in Table 2) launched by plastic balloons.

Date	Opening of launch-time window (LT = UTC + 9)			
	0530–0600	0730–0800	1500	1800
16 Feb	RS			
17 Feb	RS			
18 Feb	RS			
19 Feb				
20 Feb	RS	RS*	Payload 2	
21 Feb				
22 Feb	RS	JTBK-A		
23 Feb			Payload 2	Payload 1
24 Feb	RS	JTBK-B		
25 Feb	RS	Payload 4		Payload 1
26 Feb	RS	JTBK-C		
27 Feb			Payload 3	Payload 1
28 Feb	RS	JTBK-D		
1 Mar	RS	Payload 4	Payload 2	
2 Mar			Payload 2	Payload 1
3 Mar			Payload 1	

some instruments. The launch field constructed at Biak station is shown in the inset in Fig. 2. Unfortunately, some palm and pine trees had to be felled during construction of the launch area. However, it was sufficiently wide for plastic balloons to be laid on a groundsheet (marked as the blue-colored area in Fig. 2) during inflation. In short, the research presented interesting challenges independent of the scientific ones. Details of CUBE/Biak’s coordination may be found in Ikeda et al. (2017).

OPERATION OF CUBE/BIAK. *Background meteorological conditions.* CUBE/Biak was conducted for about 2 weeks during February–March 2015 (Table 1). The average large-scale meteorological field during CUBE/Biak is illustrated in Fig. 3 with a map of temperature and horizontal wind components at 100 hPa (top) and a longitude–pressure section of zonal anomalies of temperature and two-dimensional (zonal and vertical) wind over the equator (bottom). The bottom panel in Fig. 3 shows large-scale convective motion (a bundle of wind vectors directed upward) organized at ~160°E in the troposphere and tilted cold and warm anomalies in the lower

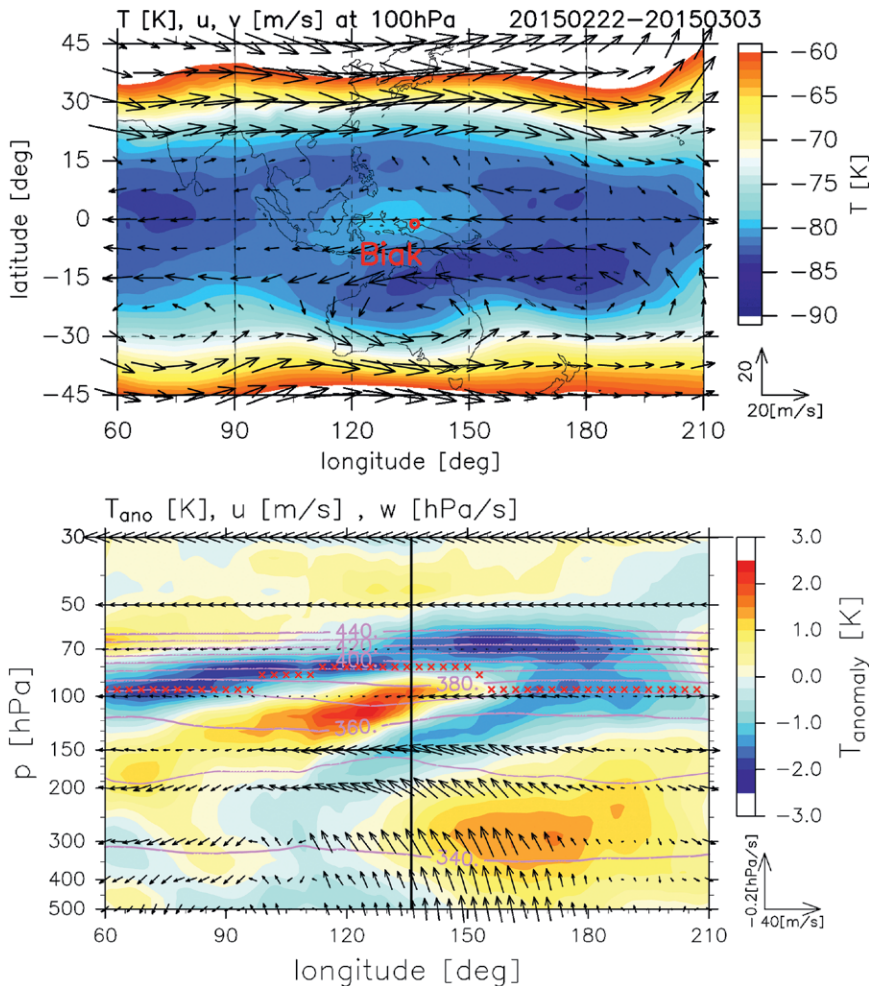


FIG. 3. (top) Longitude–latitude map of temperature (color) and horizontal wind vectors (arrows) at the 100-hPa pressure level. (bottom) Longitude–height (pressure) section of the zonal anomalies (deviations from zonal mean) of temperature (color) and zonal–vertical wind vectors (arrows) over the equator. Purple lines are contours of potential temperature. Red crosses show the location of the cold point for each longitude, while the solid line near 140°E marks the longitude of Biak. All fields are averages from 22 Feb to 3 Mar 2015 using data from ERA-Interim (Dee et al. 2011).

stratosphere and the upper troposphere over the equator (color shading). The horizontal structure (Fig. 3, top) comprises a pair of anticyclones straddling the equator (Rossby response) and a cold region over the equator to the east (Kelvin response) developing over the planetary-scale latent heating center over the western tropical Pacific. This wind and temperature pattern is the three-dimensional structure of what Newell and Gould-Stewart (1981) called the stratospheric fountain. The air, injected into the TTL by deep convection, circulates around the subtropical anticyclones while encountering low temperatures over the equator. During the course of advection, the air loses water in excess of saturation, is lifted

up gradually by radiative heating, and is finally transported to the stratosphere with the aid of the suction pump (Hatsushika and Yamazaki 2003).

Two weeks of almost-daily balloon launches alternated between instrument suites. Most launches sampled high-vertical-resolution meteorology, with supplementary data. On some nights, the supplementary payload accurately measured vapor, ozone, and cloud particles. On other days, the supplementary payload made CO₂ profiling measurements. On a few days, flasks sampled air at two altitudes for more extensive chemical analysis on the ground. These payloads are described in more detail below, and launch dates are listed in Table 1.

SOWER observations of dynamics and physics.

Vertical profiles of minor constituents, aerosols, and cloud particles along with the background meteorological fields were observed by specifically designed instruments (Table 2). Up to several instruments were connected to radiosonde(s)

to make up a payload for a rubber balloon launch. The decision to launch was made depending on weather conditions, readiness of instrument preparation, and availability of operation time. Four types of payloads were launched:

Payload 1 consisted of five types of meteorological instrument (Fig. 4, top). Simultaneous with radiosonde observations of temperature, relative humidity, and GPS position, precise values of low-concentration water vapor, ozone, and cloud particles (Vömel et al. 2007; Komhyr et al. 1995; Fujiwara et al. 2016) were measured at high vertical resolution. GPS altitude was converted to air

TABLE 2. Summary of the instrumentation used during CUBE/Biak. TA-300, TA-1200, and TA-3000 refer to rubber balloons weighing 300, 1,200, and 3,000 g, respectively. FB5B and FB9B refer to plastic balloons (see Table 4 for balloon specifications). Mole fractions are expressed in ppm and ppt corresponding to $\mu\text{mol mol}^{-1}$ and pmol mol^{-1} , respectively.

Instrument (model) [operation]	Observed quantity (unit)	Principle	Height range	Uncertainty	Reference	Application
1 Radiosonde (RS-06G, RS-11G) [TA-300, TA-1200]	Temperature ($^{\circ}\text{C}$) Relative humidity (%) Wind velocity (m s^{-1})	Thermistor Capacitance GPS	0–35 km Troposphere Troposphere, stratosphere	$<0.8^{\circ}\text{C}$ (day) $<0.4^{\circ}\text{C}$ (night) $<7\%$ $<2 \text{ m s}^{-1}$ $<3 \text{ m s}^{-1}$	www.meisei.co.jp/english/products/meteo/ ; Nash et al. (2011)	Upper-air meteorological conditions
2 Ozone sonde (1ZECC) [TA-1200]	O_3 partial pressure (mPa)	Electrochemical concentration cell	0–35 km	$<3\%$ (100–10 hPa)	Komhyr et al. (1995)	Troposphere–stratosphere exchange
3 Water vapor sonde (CFH) [TA-1200]	Frost point temperature ($^{\circ}\text{C}$)	Cryogenic frost point hygrometer	0–35 km	$<10\%$	Vömel et al. (2007, 2016)	Dehydration; water vapor tape recorder
4 CO_2 sonde (MCD-10) [TA-300]	CO_2 mole fraction (ppm)	Nondispersive infrared absorption	0–5 km 5–10 km	<1 (ppm) <1.5 (ppm)	www.meisei.co.jp/english/products/meteo/	Tropospheric transport
5 Cloud particle sensor (CPS) [TA-1200]	Particle counts (s^{-1}) Degree of polarization	Diode laser (790 nm)	0–20 km	Section 2.3 in Fujiwara et al. (2016) Section 2.1 in Fujiwara et al. (2016)	Fujiwara et al. (2016)	Ice particle formation
6 Optical particle counter (OPC) [TA-3000]	Size-classified (0.3–11.7 μm) particle counts (s^{-1})	Diode laser (780 nm)	0–32 km	Appendix A in Iwasaki et al. (2007)	Iwasaki et al. (2007); Shibata et al. (2012)	Aerosol size distribution and volatility
7 Aerosol sampler (ASS) [TA-3000]	Aerosol samples ($>0.2 \mu\text{m}$)	Impaction method	10–25 km	—	M. Hayashi et al. (2018, unpublished manuscript)	Morphologies and elemental compositions of aerosols
8 Cryogenic whole-air sampler (Joule-Thompson sampler) [FB5B, FB9B]	Mole fractions of CO_2 (ppm) and SF_6 (ppt) $\delta^{15}\text{N}$, $\delta^{18}\text{O}$, $\delta(\text{Ar}/\text{N}_2)$ (meg^{-1}) Isotopocules of N_2O (mil^{-1})	Nondispersive infrared gas analyzer; gas chromatograph Mass spectrometer	16–35 km	$<0.08\%$ (CO_2) $<1.1\%$ (SF_6) $<7 \text{ meg}^{-1}$ $<0.5 \text{ mil}^{-1}$	Morimoto et al. (2009); Nakazawa et al. (1995); Aoki et al. (2003); Sugawara et al. (2018) Ishidoya et al. (2008, 2013); Sugawara et al. (2018) Toyoda et al. (2018)	Age of air; gravitational separation; isotopocules
9 Mie lidar [continuous]	Backscattering coefficient; depolarization ratio	Neodymium-doped yttrium aluminum garnet (Nd:YAG) laser (1,064 and 532 nm)	1–25 km	Section 4.3 in Shibata et al. (2012)	Shibata et al. (2012)	Observations of cirrus and aerosols over the station



FIG. 4. (top) Payload 1 comprises a cryogenic frost point hygrometer (CFH) water vapor sonde, an electrochemical concentration cell (ECC) ozonesonde with an RS-06G radiosonde, and a CPS with an RS-11G radiosonde (viewed from left to right). **(middle) Payload 2** comprises a CO₂ sonde with an RS-06G radiosonde attached to the standard gas storage box. **(bottom) Payload 3** comprises an OPC sonde (front left) connected to a thermodenuder (rear right) used to evaporate volatile aqueous aerosols.

pressure with the hypsometric equation using temperature and humidity profiles and surface pressure. Payload 1 launches were at 1800 local time (LT) to avoid solar illumination effects on the instrumentation during the ~2-h flight time.

Payload 2 comprised two CO₂ sondes, one from Japan (M. Ouchi et al. 2018, unpublished manuscript; Fig. 4, middle) and the other an experimental package from LAPAN, to observe tropospheric CO₂ profiles. Payload 2 launches took place at 1500 LT so that the flights ended before the launch of payload 1. The mole fraction was approximately constant within the range 400 ± 2 ppm up to ~10 km (Y. Inai et al. 2017, manuscript submitted to *Atmos. Environ.*).

Payload 3 comprised two optical particle counters in tandem (T-OPC). Each OPC is capable of measuring the size distribution of particles with diameter 0.3–11.7 μm (Iwasaki et al. 2007; Shibata et al. 2012). One of the two OPCs was equipped with a thermodenuder, installed on the air inlet and heated to 300°C, to measure nonvolatile particles only (Fig. 4, bottom).

Payload 4 was an aerosol sampling sonde (ASS). It collects particles >0.2 μm in diameter using an inertial impaction method (M. Hayashi et al. 2018, unpublished manuscript). Payload 4 is different from other SOWER payloads in that it must be recovered for laboratory analysis of collected samples. Two ASSs were launched by rubber balloons. During ascent, they took 13 samples between 10 and 23 km on 25 February and 15 samples between 10 and 25 km on 1 March. The sondes separated automatically from the launch balloons at a preplanned altitude and were successfully recovered at sea about 50 km west of the launch site (see the “CAS observations of transport and chemistry” section below for recovery operations). The morphologies and elemental compositions of the samples were analyzed using a scanning electron microscope and energy dispersive X-ray analyzer. These analyses provide information on aerosol size, phase, mixing state, and so on, as well as the main aerosol composition such as sulfuric acid and sulfate.

The observed data from payload 1 on 2 March are shown in Fig. 5, which illustrates vertical profiles of the ozone (green) and water vapor (red) mixing ratios and saturation mixing ratio (blue) in the left

panel. Those of zonal (red) and meridional (blue) wind components and temperature (black) are shown in the right panel. There is an inversion layer between 15 and 16 km, where the ozone and the water vapor mixing ratios exhibit positive and negative jumps, respectively, and the wind components show stepwise changes indicating a termination of the upper-tropospheric easterly shear and a reversal to a westerly shear. The layer just above this inversion with a thickness of ~ 1 km has stratospheric characteristics (i.e., ozone rich and water poor) suggestive of downward displacement associated with a large-scale wave (Fig. 3, bottom). The water vapor mixing ratio shows saturation between 17 and 18 km with slight supersaturation near 18 km. Unfortunately, ice nucleation in this layer was not confirmed by cloud particle sensor (CPS) observations as they were missing for this flight. The unsaturated air between 18 and 19 km showing a minimum of < 2 ppmv (saturation point < 185 K) must have passed an extremely cold region upstream and to the east (Fig. 3, top). Above this layer, the air temperature as well as the water and ozone mixing ratios increase steeply to stratospheric values.

The stratospheric water vapor shows a maximum at around 21 km and a secondary minimum at around 25 km. These maximum and minimum values are interpreted as the imprint of the TTL temperature in the previous Northern Hemisphere summer and winter, respectively. The real-time profile of the atmospheric tape recorder thus revealed has been used to determine the altitude at which cryogenic air sampling should be made.

A Mie scattering depolarization lidar system (Shibata et al. 2012) was operated continuously during 18–28 February. Mass concentration and size information of the particles can be inferred from the observed backscattering coefficient at 532- and 1,064-nm wavelengths, and particle shape information (i.e., either spherical or nonspherical) can be obtained from the depolarization data at 532 nm. The complementary continuous operation of remote sensing lidar and intermittent in situ observations by CPS sondes monitored ice nucleation processes

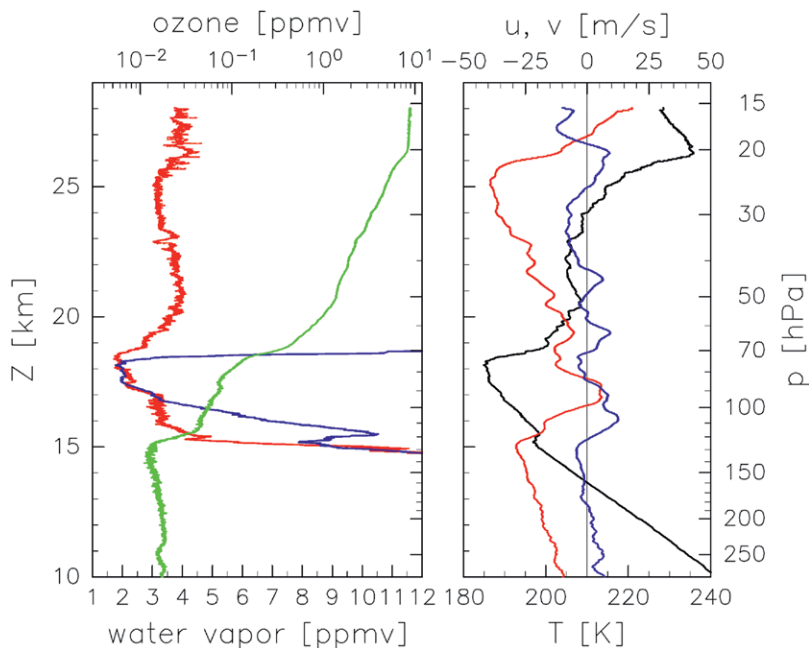


FIG. 5. Vertical profiles of (left) ozone (green), water (red), and water saturation (blue) mixing ratios (ppmv), with (right) zonal (red) and meridional (blue) wind components ($m s^{-1}$) and temperature (black; K), observed on 2 Mar 2015 over Biak.

in TTL dehydration. Fujiwara et al. (2016) presented the profiles obtained from two of the four CPS flights. For the 27 February case, CPS data showed reasonable agreement with the lidar measurements.

CAS observations of transport and chemistry. The core of CUBE/Biak is one of the first attempts at stratospheric whole-air sampling in the tropics where tropospheric air enters the stratosphere. Collected air samples are analyzed to determine accurate concentrations of CO_2 and SF_6 for estimation of AoA (Sugawara et al. 2018) and N_2O isotopocules (Toyoda et al. 2018). Concentrations of major isotopes are closely determined for quantification of gravitational separation (Sugawara et al. 2018). The species that have been analyzed to date are summarized in Table 2.

A schematic of stratospheric air sampling is shown in Fig. 6. The position and status of the sampler, transmitted by an onboard radio transmitter, were received at the LAPAN Biak station. After completion of air sampling, the instrument gondola was separated from the balloon by a rope cutter and was parachuted down to the sea for recovery by a speedboat. To ensure flawless recovery even in the event of transmitter malfunction and unpredictable drift on the sea, each gondola was equipped with an iridium buoy that disseminated its position via a satellite link and Internet connection.

Projected balloon flight trajectories were calculated in advance based on observations of the Indonesian Meteorological, Climatological, and Geophysical Agency at the Biak station. It was found that weak surface westerly and tropospheric easterly winds prevail in the early morning during February–March. In some cases, inflows and outflows associated with large convective systems nearby could deflect the trajectories in a north–south direction. The stratospheric quasi-biennial oscillation showed a weak

westerly maximum in the lower stratosphere and an easterly maximum at around 25 km in early 2015. The alternation of the zonal wind was helpful for ensuring a splashdown near the launch site.

Four air-sampling experiments were performed using polyethylene film balloons. The payload consisted of a timer, two rope cutters, a flasher, a parachute, an instrument gondola, and an iridium buoy (Fig. 7). Each instrument gondola was equipped with two air samplers. Each sampler collected an air

sample at a different pre-assigned altitude between the TTL and 30 km above sea level (Table 3). Thus, a profile consisting of air samples from eight altitudes was obtained. Figure 8 shows the air-sampling system that comprised the cryogenic air samplers and peripheral devices including a controller unit with a GPS receiver and a telemetry transmitter. The cryogenic air sampler used a cooling device called the Joule–Thomson minicooler to solidify or liquefy almost all atmospheric constituents (Morimoto et al. 2009). The dimensions of

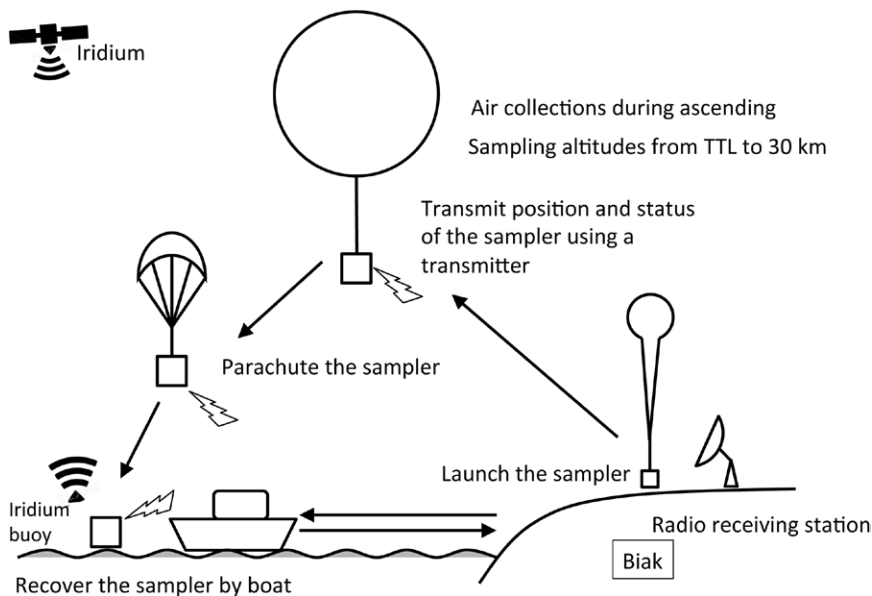


FIG. 6. Schematic of stratospheric air sampling.

TABLE 3. Sampling altitudes and sampled amounts of air for cryogenic samplers. See Table 4 for balloon specifications.

Date	Sampler	Balloon	Launch–landing time (LT)	Landing position	Sampling altitude (km)	Sampled amount (L–STP)
22 Feb	JTBK-A	FB5B	0810–0940	1°1'41"S, 135°35'6"E	16.52–17.94	7.6
					19.94–21.71	0.8
24 Feb	JTBK-B	FB5B	0800–0941	1°8'41"S, 135°36'25"E	17.71–19.27	9.3
					21.10–22.95	6.9
26 Feb	JTBK-C	FB9B	0727–0930	1°10'58"S, 135°30'19"E	22.91–24.85	6.9
					26.21–28.65	7.7
28 Feb	JTBK-D	FB9B	0720–0926	1°3'40"S, 135°34'19"E	24.06–26.42	7.3
					27.33–30.04	2.0

TABLE 4. Dimensions and weights of plastic balloons used for cryogenic air sampling.

	Volume of full expansion (m ³)	Max diameter (m)	Max length (m)	Weight (kg)
FB5B	5,000	22.6	33.5	39
FB9B	9,000	25.8	39.8	57

the instrument gondola equipped with two samplers were 60 cm × 35 cm × 75 cm (length × width × height) and its total weight was about 40 kg. Two types of balloon (i.e., FB5B and FB9B) were used (Table 4), reflecting the constraints of efficient use of consumables (balloons and helium gas) at designated sampling altitudes.

The launching operation relied on the latest prediction of the balloon trajectory provided by the support team of the Institute of Space and Astronautical Science's (ISAS) Balloon Engineering Group (Japan) via email. The calculation employed Global Forecast System (GFS) data published by the National Centers for Environmental Information. Additional effort was made to estimate the range of uncertainty regarding the splashdown sites using GFS 24-h ensemble forecasts. Unfortunately, the ensemble trajectories could not be used in real-time operations because of limited Internet connectivity. Launches occurred only when the splashdown of the balloon was predicted to be west of the island of Biak and within reach (~70 km) of a recovery boat. For safety reasons, balloons were not flown over land, except for the few moments immediately following the launch.

Flight plans determining suitable combinations of balloon size and sampling altitudes were designed on site based on a complete assessment of the experimental conditions (i.e., upper-atmospheric wind, ground weather conditions, and sea surface conditions). Balloon launch operations were undertaken by 15–16 persons referring to the carefully preplanned launch sequence (Fig. 9) so that the balloons could be launched safely even by inexperienced persons without the use of heavy vehicles. From the moment of the decision to launch, it took approximately 90 min to release a balloon. This included transportation of the balloon and instrument gondola to the launch site, preparation of the cryogenic sampler, and inflation of the balloon with the helium gas.

Flight trajectories of all four flights are shown in the top panel in Fig. 10. Stratospheric air sampling was conducted during the ascending phase of the flights (Table 3; Fig. 10, bottom). Splashdown times and positions together with the amount of sampled air are summarized in Table 3. Recovery operations were successfully conducted by a chartered speedboat and collaborating officers from the local marine police. During operations, the GPS position of the instrument gondola, transmitted by the iridium buoy, was reported frequently from the LAPAN Biak station to the recovery team using cellular telephones, UHF radio communication, or iridium telephone. With the GPS information, as well as radio direction

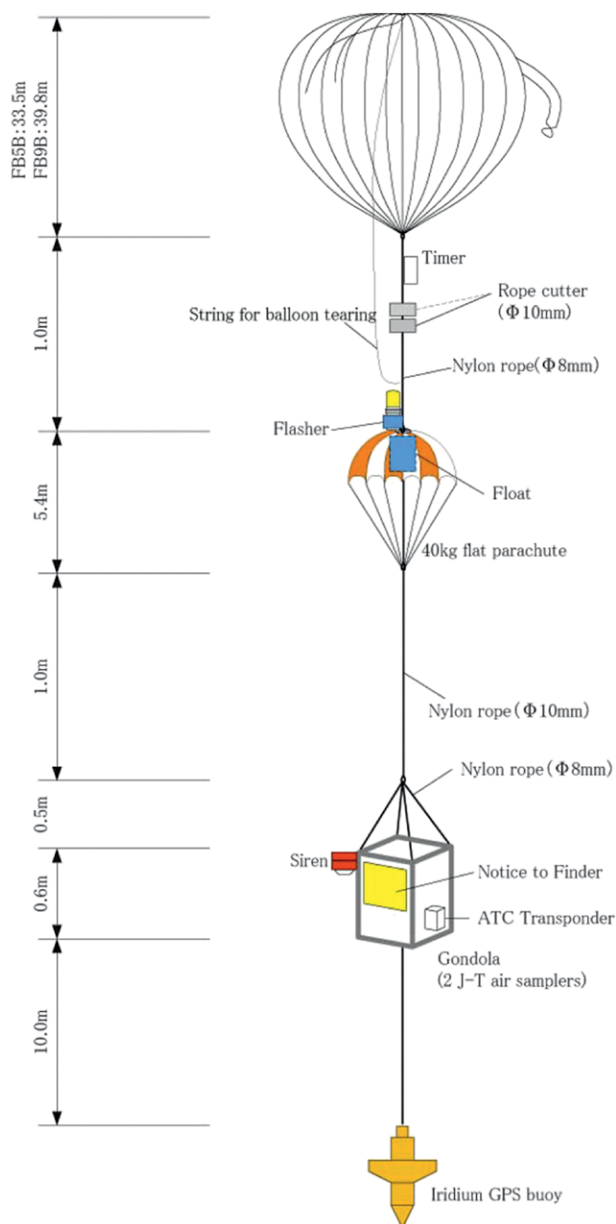


Fig. 7. Balloon and payload of the air sampling system.

measurements undertaken on the boat, the recovery team was able to locate the gondola within 30–60 min after splashdown. All samplers were waterproof and were prepared for the impact of splashdown into the sea. Unfortunately, however, one sampler assigned to 21–22 km leaked after landing because of trouble with its electrical circuit.

DISCUSSION. We have focused on the tropical stratosphere with the intention of distinguishing individual contributing processes. The focus on the tropics has another advantage in the use of the water vapor tape recorder, together with AoA, to

independently quantify the stratospheric transit time (see the “Why do we need CUBE/Biak?” section). However, the mean age estimated from CO₂ disagreed with the phase delay in the water vapor tape recorder (Vaugh and Hall 2002). To investigate the processes responsible for creating such a difference, it is interesting to estimate both variables simultaneously using

a single meteorological dataset and to compare them with the CUBE/Biak observations.

Figure 11 compares the vertical profiles of CO₂ (Fig. 11a) and SF₆ (Fig. 11b) mole fractions, mean age (Fig. 11c), and water vapor mixing ratio (Fig. 11d) estimated from CUBE/Biak observations with those derived by backward trajectory calculations

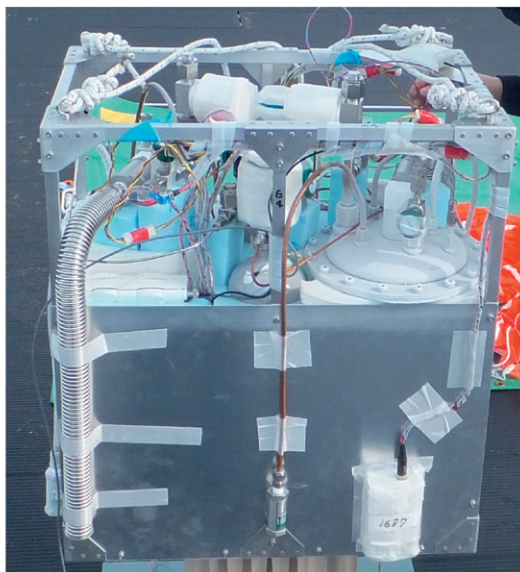
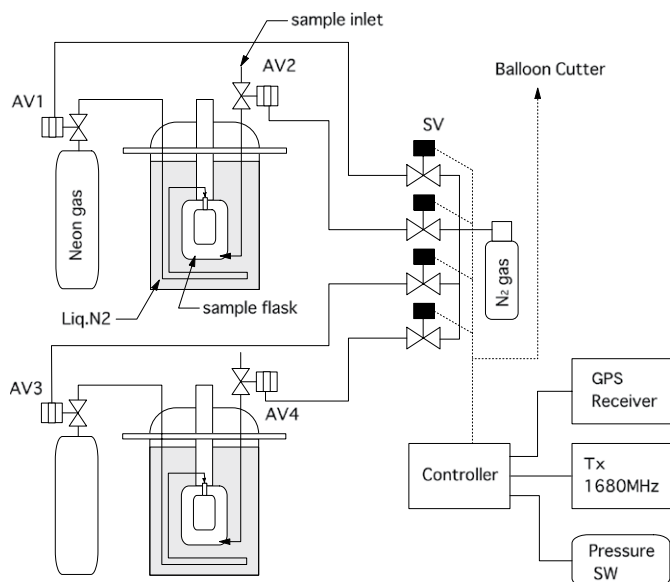


FIG. 8. (left) Schematic of the balloonborne air sampling system. The solenoid and pneumatic valves are indicated by SV and AV, respectively. A sample flask was set in a Dewar flask filled with LN. The Joule–Thomson minicooler was fixed in the sample flask. (right) A photograph of the air sampling system. Two air samplers were assembled inside of one instrument gondola.

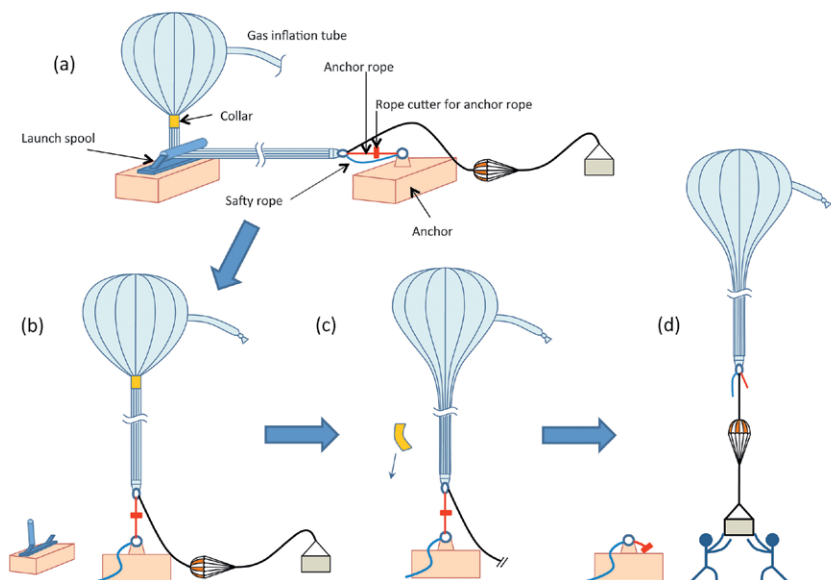


FIG. 9. (left) Stages of the launch procedure. (a) The balloon bottom is held by an anchor during gas inflation. (b) After gas inflation, the balloon is raised by opening the spool and removing the safety rope. (c) The collar is released. (d) The balloon is launched by cutting the anchor rope. (right) A snapshot showing the balloon launch for cryogenic air sampling at Biak on 24 Feb 2015.

(appendix on “Trajectory calculations”). Colored crosses and horizontal bars represent the mean and uncertainty, respectively, from air samples (Sugawara et al. 2018) while the red line is the observed water vapor profile (Fig. 5). Black crosses are the estimates from trajectory calculations. The vertical bars indicate the height ranges in which air samples are taken. It is evident that the upward tracer transport estimated by trajectories is too fast, leading to a smaller rate of decrease with height for both CO_2 and SF_6 mole

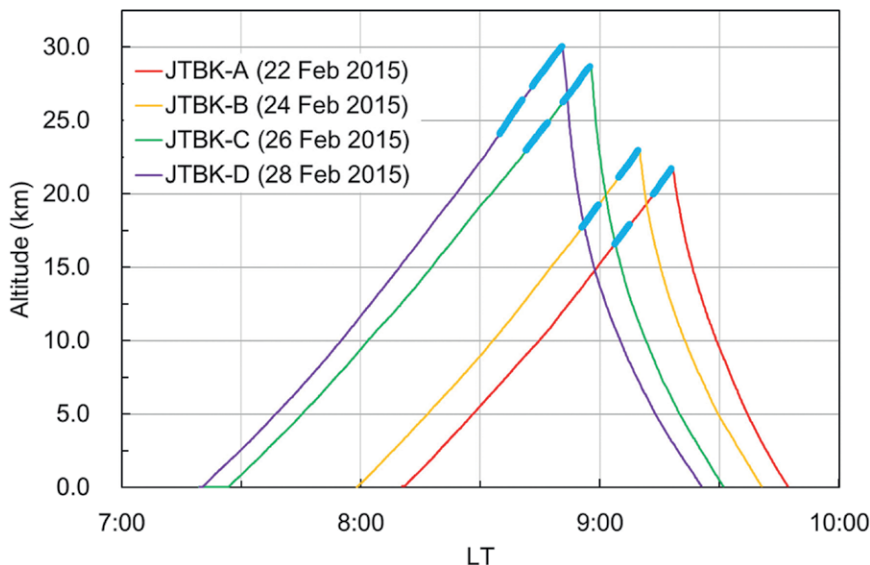
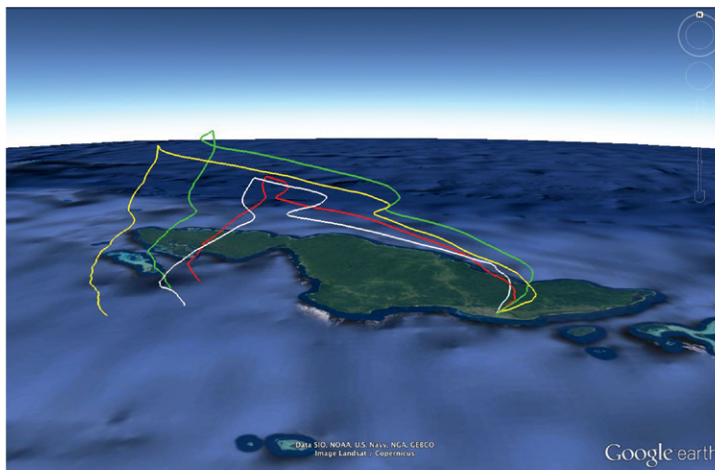


FIG. 10. (top) Bird's-eye view of Biak and 3D balloon trajectories for the four cryogenic samplers (red, JTBK-A; white, JTBK-B; yellow, JTBK-C; and green, JTBK-D). (bottom) Time (LT)–height (km) plot for air samplers. Thick blue portions indicate sampling positions where an inlet valve was open.

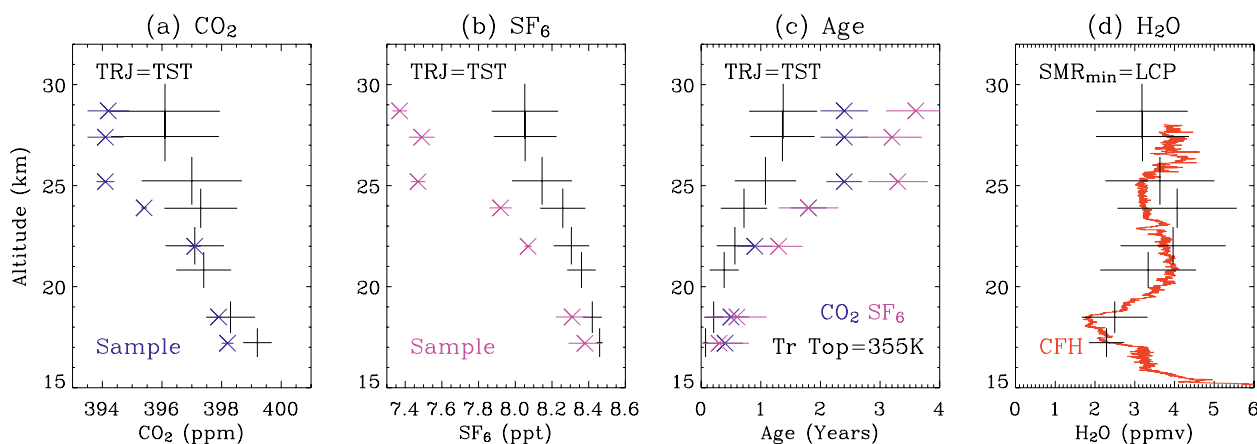


FIG. 11. Vertical profiles of mole fractions of (a) CO_2 (ppm) and (b) SF_6 (ppt), (c) mean age (yr), and (d) water vapor mixing ratio (ppmv). Those shown in color are observational estimates from air samples (Sugawara et al. 2018), while the red line shows the observed water vapor profile depicted in Fig. 5. Black crosses are the estimates from trajectory calculations corresponding to CUBE/Biak. The horizontal bars are the intervals of uncertainty expressed as one standard deviation, while the vertical bars are the ranges for air sampling and the initialization height for trajectory calculations.

fractions, a younger age, and higher rate of ascent of the tape recorder signal than observed. The differences appear to be too large to be explained solely by a truncation ($\leq 1,200$ days) of age spectra. Instead, they may be related to the dynamical field used in the trajectory calculations. Actually, Glanville and Birner (2017) pointed out that the vertical velocities in the European Centre for Medium-Range Weather Forecasts (ECMWF) interim reanalysis (ERA-Interim) are 2–4 times greater than those estimated from the water vapor tape recorder in satellite data. In spite of the shortcomings of the present calculations, it is interesting to note that the mean age and the mole fractions of CO_2 and SF_6 are nearly constant above 25 (27) km in air samples (trajectory calculations). The contributions of vertical and horizontal mixing and transport (Ploeger et al. 2010, 2012), including the excessive vertical dispersion that results from the use of assimilated meteorological fields in the kinematic trajectories (Schoeberl et al. 2003), need to be quantified carefully. Gravitational separation (Sugawara et al. 2018) and N_2O isotopocules (Toyoda et al. 2018) will provide independent information to help decouple these entangled contributing factors.

CONCLUDING REMARKS. CUBE/Biak, aimed at achieving a synthesized view of the dynamics and chemistry of the tropical stratosphere and the TTL, was completed successfully despite numerous legal and technical difficulties. Air samples collected by cryogenic sampling were analyzed for various greenhouse gases and their isotopes to derive a vertical profile of the AoA inside the tropical pipe. The water vapor tape recorder, observed by frost point hygrometer sondes, proved useful as an independent measure of the elapsed time since the air entered the stratosphere. Detailed analyses are currently being performed to extend the original campaign's scope to other related issues, for example, stratospheric age spectra, gravitational separation, and N_2O isotopocules. A similar campaign, to be undertaken during boreal summer, will provide further insights into mixing from the midlatitudes.

ACKNOWLEDGMENTS. We would like to express our gratitude to the members of the Scientific Ballooning (DAIKIKYU) Research and Operation Group and M. Fujimoto of ISAS, JAXA. We would also like to thank colleagues at LAPAN, Indonesia, especially C. Dewanto, A. Hidayat, and T. Djamaluddin; members of Marine Polisi Indonesia stationed at Biak; F. Helfi of PT. Mahkota Logistik Indoraya; S. Ishikawa of Samator Group, PT.

Aneka Industri; S. Wahyono of RISTEK, Indonesia; and H. Hikita of the Indonesian Embassy in Tokyo. Thanks are also due to S. Saraspriya for his assistance. We appreciate three anonymous reviewers and B. Mapes, responsible editor, for helpful and constructive comments that greatly improved this manuscript. This work was supported by the Japan Society for the Promotion of Science, Grant-in-Aid for Scientific Research (S) 26220101, and it was also selected and supported as a Small-Size Project by ISAS, JAXA.

APPENDIX: ADDITIONAL INFORMATION ON LEGAL ISSUES. An FRP application is initiated by submitting appropriate documentation to RISTEK and the Indonesian representative (embassy or consulate general) in the home country of the applicant. The FRP secretariat invites Indonesian research counterparts authorized by an official agreement to attend a meeting to explain the purpose of the intended research. Once approved, a foreign researcher (FR) is granted a visa 315 by the Indonesian representative in his or her home country. Upon arrival in Jakarta, an FR must report to the FRP secretariat in the RISTEK office to receive the research permit and other related documents. Next, an FR must visit the police headquarters, Ministry of Home Affairs, and immigration office to obtain a traveling permit, research notification, and limited-stay permit card, respectively. Upon arrival in Biak, an FR should report to both the local immigration office to obtain another limited-stay permit card and the provincial police headquarters to obtain a certificate of police registration card.

A notice to airmen (NOTAM) application should be submitted at least one month in advance of the operation and each balloon launch must be reconfirmed one day before. LAPAN also coordinated with the air traffic controller (ATC) of Biak International Airport. The provisions of International Civil Aviation Organization (ICAO) rules are as follows:

- 1) The balloon envelope contains radar-reflective material.
- 2) The balloon system is equipped with an ATC transponder.
- 3) The balloon system is equipped with two rope cutters to be used as flight-termination devices that are operated independently by an onboard control device and timer.

As the Biak ATC could not receive the payload transponder signal, LAPAN sent a representative to Biak International Airport to advise the ATC of the

payload position every 2 min until splashdown. The gondola had to be equipped with a flasher to provide a warning to persons close to the landing position.

APPENDIX: TRAJECTORY CALCULATIONS. Backward trajectory calculations are conveniently used to estimate the transport of tracers from the troposphere to the stratosphere (e.g., Fueglistaler et al. 2005). Kinematic backward trajectories are calculated for 1,200 days to estimate the time of entry to the stratosphere and the minimum saturation mixing ratio of water at the Lagrangian cold point (LCP; SMR_{min}) for air parcels observed during CUBE/Biak. In this preliminary analysis, calculations are made by using low-resolution ERA-Interim pressure-level data for the sake of computational efficiency. Trajectories are initialized at altitudes in each of the sampling ranges (Table 3) with 100-m increments so that the trajectory analysis reflects the vertical range of the sampled air. In these calculations, only the troposphere-to-stratosphere transport (TST) trajectories are used, that is, the trajectories traceable down to 340 K recording an SMR_{min} in the TTL. Here, the TTL is defined as the layer between the isentropic levels of 355 and 400 K between 30°N and 30°S (Hasebe and Noguchi 2016). Air parcels are assumed to retain the SMR_{min} at the LCP and the mole fractions of CO_2 and SF_6 of the tropical upper troposphere, as compiled by Sugawara et al. (2018), at the time of the final passage through the 355-K isentropic surface, when the count of the age commences.

REFERENCES

- Andrews, D. G., and M. E. McIntyre, 1976: Planetary waves in horizontal and vertical shear: The generalized Eliassen–Palm relation and the mean zonal acceleration. *J. Atmos. Sci.*, **33**, 2031–2048, [https://doi.org/10.1175/1520-0469\(1976\)033<2031:PWIHAV>2.0.CO;2](https://doi.org/10.1175/1520-0469(1976)033<2031:PWIHAV>2.0.CO;2).
- Aoki, S., and Coauthors, 2003: Carbon dioxide variations in the stratosphere over Japan, Scandinavia and Antarctica. *Tellus*, **55B**, 178–186, <https://doi.org/10.3402/tellusb.v55i2.16750>.
- Atticks, M. G., and G. D. Robinson, 1983: Some features of the structure of the tropical tropopause. *Quart. J. Roy. Meteor. Soc.*, **109**, 295–308, <https://doi.org/10.1002/qj.49710946004>.
- Austin, J., J. Wilson, F. Li, and H. Vömel, 2007: Evolution of water vapor concentrations and stratospheric age of air in coupled chemistry–climate model simulations. *J. Atmos. Sci.*, **64**, 905–921, <https://doi.org/10.1175/JAS3866.1>.
- Banks, P. M., and G. Kockarts, 1973a: *Aeronomy: Part A*. Academic Press, 430 pp.
- , and —, 1973b: *Aeronomy: Part B*. Academic Press, 355 pp.
- Brewer, A. W., 1949: Evidence for a world circulation provided by the measurements of helium and water vapour distribution in the stratosphere. *Quart. J. Roy. Meteor. Soc.*, **75**, 351–363, <https://doi.org/10.1002/qj.49707532603>.
- Dee, D. P., and Coauthors, 2011: The ERA-Interim reanalysis: Configuration and performance of the data assimilation system. *Quart. J. Roy. Meteor. Soc.*, **137**, 553–597, <https://doi.org/10.1002/qj.828>.
- Diallo, M., B. Legras, and A. Chédin, 2012: Age of stratospheric air in the ERA-Interim. *Atmos. Chem. Phys.*, **12**, 12 133–12 154, <https://doi.org/10.5194/acp-12-12133-2012>.
- Dobson, G. M. B., 1956: Origin and distribution of the polyatomic molecules in the atmosphere. *Proc. Roy. Soc. London*, **236A**, 187–193, <https://doi.org/10.1098/rspa.1956.0127>.
- Engel, A., and Coauthors, 2009: Age of stratospheric air unchanged within uncertainties over the past 30 years. *Nat. Geosci.*, **2**, 28–31, <https://doi.org/10.1038/ngeo388>.
- Fueglistaler, S., M. Bonazzola, P. H. Haynes, and T. Peter, 2005: Stratospheric water vapor predicted from the Lagrangian temperature history of air entering the stratosphere in the tropics. *J. Geophys. Res.*, **110**, D08107, <https://doi.org/10.1029/2004JD005516>.
- , A. E. Dessler, T. J. Dunkerton, I. Folkins, Q. Fu, and P. W. Mote, 2009: Tropical tropopause layer. *Rev. Geophys.*, **47**, RG1004, <https://doi.org/10.1029/2008RG000267>.
- Fujiwara, M., F. Hasebe, M. Shiotani, N. Nishi, H. Vömel, and S. J. Oltmans, 2001: Water vapor control at the tropopause by equatorial Kelvin waves observed over the Galápagos. *Geophys. Res. Lett.*, **28**, 3143–3146, <https://doi.org/10.1029/2001GL013310>.
- , and Coauthors, 2010: Seasonal to decadal variations of water vapor in the tropical lower stratosphere observed with balloon-borne cryogenic frost point hygrometers. *J. Geophys. Res.*, **115**, D18304, <https://doi.org/10.1029/2010JD014179>.
- , and Coauthors, 2016: Development of a cloud particle sensor for radiosonde sounding. *Atmos. Meas. Tech.*, **9**, 5911–5931, <https://doi.org/10.5194/amt-9-5911-2016>.
- Garcia, R. R., and W. J. Randel, 2008: Acceleration of the Brewer–Dobson circulation due to increases in greenhouse gases. *J. Atmos. Sci.*, **65**, 2731–2739, <https://doi.org/10.1175/2008JAS2712.1>.

- , —, and D. E. Kinnison, 2011: On the determination of age of air trends from atmospheric trace species. *J. Atmos. Sci.*, **68**, 139–154, <https://doi.org/10.1175/2010JAS3527.1>.
- Gill, A. E., 1980: Some simple solutions for heat-induced tropical circulation. *Quart. J. Roy. Meteor. Soc.*, **106**, 447–462, <https://doi.org/10.1002/qj.49710644905>.
- Glanville, A. A., and T. Birner, 2017: Role of vertical and horizontal mixing in the tape recorder signal near the tropical tropopause. *Atmos. Chem. Phys.*, **17**, 4337–4353, <https://doi.org/10.5194/acp-17-4337-2017>.
- Hall, T. M., and R. A. Plumb, 1994: Age as a diagnostic of stratospheric transport. *J. Geophys. Res.*, **99**, 1059–1070, <https://doi.org/10.1029/93JD03192>.
- Harris, N. R. P., and Coauthors, 2017: Coordinated Airborne Studies in the Tropics (CAST). *Bull. Amer. Meteor. Soc.*, **98**, 145–162, <https://doi.org/10.1175/BAMS-D-14-00290.1>.
- Hasebe, F., and T. Noguchi, 2016: A Lagrangian description on the troposphere-to-stratosphere transport changes associated with the stratospheric water drop around the year 2000. *Atmos. Chem. Phys.*, **16**, 4235–4249, <https://doi.org/10.5194/acp-16-4235-2016>.
- , and Coauthors, 2013: Cold trap dehydration in the tropical tropopause layer characterised by SOWER chilled-mirror hygrometer network data in the tropical Pacific. *Atmos. Chem. Phys.*, **13**, 4393–4411, <https://doi.org/10.5194/acp-13-4393-2013>.
- Hatsushika, H., and K. Yamazaki, 2003: Stratospheric drain over Indonesia and dehydration within the tropical tropopause layer diagnosed by air parcel trajectories. *J. Geophys. Res.*, **108**, 4610, <https://doi.org/10.1029/2002JD002986>.
- Haynes, P. H., C. J. Marks, M. E. McIntyre, T. G. Shepherd, and K. P. Shine, 1991: On the “downward control” of extratropical diabatic circulations by eddy-induced mean zonal forces. *J. Atmos. Sci.*, **48**, 651–678, [https://doi.org/10.1175/1520-0469\(1991\)048<0651:OTCOED>2.0.CO;2](https://doi.org/10.1175/1520-0469(1991)048<0651:OTCOED>2.0.CO;2).
- Highwood, E. J., and B. J. Hoskins, 1998: The tropical tropopause. *Quart. J. Roy. Meteor. Soc.*, **124**, 1579–1604, <https://doi.org/10.1002/qj.49712454911>.
- Holton, J. R., and A. Gettelman, 2001: Horizontal transport and the dehydration of the stratosphere. *Geophys. Res. Lett.*, **28**, 2799–2802, <https://doi.org/10.1029/2001GL013148>.
- , P. H. Haynes, M. E. McIntyre, A. R. Douglass, R. B. Rood, and L. Pfister, 1995: Stratosphere-troposphere exchange. *Rev. Geophys.*, **33**, 403–439, <https://doi.org/10.1029/95RG02097>.
- Ikedo, C., and Coauthors, 2017: Stratospheric air sampling using a balloon-borne cryogenic sampler over Biak island, Indonesia (in Japanese). JAXA Research and Development Rep. JAXA-RR-16-008, 33–48, <https://doi.org/10.20637/JAXA-RR-16-008/0002>.
- Inai, Y., and Coauthors, 2018: Balloon-borne tropospheric CO₂ observations over the equatorial eastern and western Pacific. *Atmos. Environ.*, **184**, 24–36, <https://doi.org/10.1016/j.atmosenv.2018.04.016>.
- Ishidoya, S., S. Sugawara, S. Morimoto, S. Aoki, and T. Nakazawa, 2008: Gravitational separation of major atmospheric components of nitrogen and oxygen in the stratosphere. *Geophys. Res. Lett.*, **35**, L03811, <https://doi.org/10.1029/2007GL030456>.
- , —, —, —, —, H. Honda, and S. Murayama, 2013: Gravitational separation in the stratosphere—A new indicator of atmospheric circulation. *Atmos. Chem. Phys.*, **13**, 8787–8796, <https://doi.org/10.5194/acp-13-8787-2013>.
- Iwasaki, S., and Coauthors, 2007: Characteristics of aerosol and cloud particle size distributions in the tropical tropopause layer measured with optical particle counter and lidar. *Atmos. Chem. Phys.*, **7**, 3507–3518, <https://doi.org/10.5194/acp-7-3507-2007>.
- Jensen, E. J., and Coauthors, 2017: The NASA Airborne Tropical Tropopause Experiment: High-altitude aircraft measurements in the tropical western Pacific. *Bull. Amer. Meteor. Soc.*, **98**, 129–143, <https://doi.org/10.1175/BAMS-D-14-00263.1>.
- Kida, H., 1983: General circulation of air parcels and transport characteristics derived from a hemispheric GCM. Part 2: Very long-term motions of air parcels in the troposphere and stratosphere. *J. Meteor. Soc. Japan*, **61**, 510–523, https://doi.org/10.2151/jmsj1965.61.4_510.
- Komala, N., S. Saraspriya, K. Kita, and T. Ogawa, 1996: Tropospheric ozone behavior observed in Indonesia. *Atmos. Environ.*, **30**, 1851–1856, [https://doi.org/10.1016/1352-2310\(95\)00382-7](https://doi.org/10.1016/1352-2310(95)00382-7).
- Komhyr, W. D., R. A. Barnes, G. B. Brothers, J. A. Lathrop, and D. P. Opperman, 1995: Electrochemical concentration cell ozonesonde performance evaluation during STOIC 1989. *J. Geophys. Res.*, **100**, 9231–9244, <https://doi.org/10.1029/94JD02175>.
- Matsuno, T., 1966: Quasi-geostrophic motions in the equatorial area. *J. Meteor. Soc. Japan*, **44**, 25–43, https://doi.org/10.2151/jmsj1965.44.1_25.
- McLandress, C., and T. G. Shepherd, 2009: Simulated anthropogenic changes in the Brewer–Dobson circulation, including its extension to high latitudes. *J. Climate*, **22**, 1516–1540, <https://doi.org/10.1175/2008JCLI2679.1>.
- Morimoto, S., and Coauthors, 2009: A new compact cryogenic air sampler and its application in stratospheric greenhouse gas observation at Syowa Station,

- Antarctica. *J. Atmos. Oceanic Technol.*, **26**, 2182–2192, <https://doi.org/10.1175/2009JTECHA1283.1>.
- Mote, P. W., and Coauthors, 1996: An atmospheric tape recorder: The imprint of tropical tropopause temperatures on stratospheric water vapor. *J. Geophys. Res.*, **101**, 3989–4006, <https://doi.org/10.1029/95JD03422>.
- Nakazawa, T., T. Machida, S. Sugawara, S. Murayama, S. Morimoto, G. Hashida, H. Honda, and T. Itoh, 1995: Measurements of the stratospheric carbon dioxide concentration over Japan using a balloon-borne cryogenic sampler. *Geophys. Res. Lett.*, **22**, 1229–1232, <https://doi.org/10.1029/95GL01188>.
- , and Coauthors, 2002: Variations of stratospheric trace gases measured using a balloon-borne cryogenic sampler. *Adv. Space Res.*, **30**, 1349–1357, [https://doi.org/10.1016/S0273-1177\(02\)00551-3](https://doi.org/10.1016/S0273-1177(02)00551-3).
- Nash, J., T. Oakley, H. Vömel, and L. Wei, 2011: WMO Intercomparison of high quality radiosonde systems: Yangjiang, China, 12 July–3 August 2010. World Meteorological Organization Instruments and Observing Methods Rep. 107, 238 pp., https://library.wmo.int/pmb_ged/wmo-td_1580.pdf.
- Newell, R. E., and S. Gould-Stewart, 1981: A stratospheric fountain? *J. Atmos. Sci.*, **38**, 2789–2796, [https://doi.org/10.1175/1520-0469\(1981\)038<2789:ASF>2.0.CO;2](https://doi.org/10.1175/1520-0469(1981)038<2789:ASF>2.0.CO;2).
- Noersomadi, and T. Tsuda, 2017: Comparison of three retrievals of COSMIC GPS radio occultation results in the tropical upper troposphere and lower stratosphere. *Earth, Planets Space*, **69**, 125, <https://doi.org/10.1186/s40623-017-0710-7>.
- Oigawa, M., T. Matsuda, T. Tsuda, and Noersomadi, 2017: Coordinated observation and numerical study on a diurnal cycle of tropical convection over a complex topography in West Java, Indonesia. *J. Meteor. Soc. Japan*, **95**, 261–281, <https://doi.org/10.2151/jmsj.2017-015>.
- Oman, L., D. W. Waugh, S. Pawson, R. S. Stolarski, and P. A. Newman, 2009: On the influence of anthropogenic forcings on changes in the stratospheric mean age. *J. Geophys. Res.*, **114**, D03105, <https://doi.org/10.1029/2008JD010378>.
- Pan, L. L., and Coauthors, 2017: The Convective Transport of Active Species in the Tropics (CONTRAST) experiment. *Bull. Amer. Meteor. Soc.*, **98**, 106–128, <https://doi.org/10.1175/BAMS-D-14-00272.1>.
- Park, S., and Coauthors, 2007: The CO₂ tracer clock for the tropical tropopause layer. *Atmos. Chem. Phys.*, **7**, 3989–4000, <https://doi.org/10.5194/acp-7-3989-2007>.
- Ploeger, F., P. Konopka, G. Günther, J.-U. Groöf, and R. Müller, 2010: Impact of the vertical velocity scheme on modeling transport in the tropical tropopause layer. *J. Geophys. Res.*, **115**, D03301, <https://doi.org/10.1029/2009JD012023>.
- , and Coauthors, 2012: Horizontal transport affecting trace gas seasonality in the tropical tropopause layer (TTL). *J. Geophys. Res.*, **117**, D09303, <https://doi.org/10.1029/2011JD017267>.
- , M. Riese, F. Haenel, P. Konopka, R. Müller, and G. Stiller, 2015: Variability of stratospheric mean age of air and of the local effects of residual circulation and eddy mixing. *J. Geophys. Res. Atmos.*, **120**, 716–733, <https://doi.org/10.1002/2014JD022468>.
- Plumb, R. A., 1996: A “tropical pipe” model of stratospheric transport. *J. Geophys. Res.*, **101**, 3957–3972, <https://doi.org/10.1029/95JD03002>.
- , 2002: Stratospheric transport. *J. Meteor. Soc. Japan*, **80**, 793–809, <https://doi.org/10.2151/jmsj.80.793>.
- Schafer, R., S. K. Avery, and K. S. Gage, 2003: A comparison of VHF wind profiler observations and the NCEP–NCAR reanalysis over the tropical Pacific. *J. Appl. Meteor.*, **42**, 873–889, [https://doi.org/10.1175/1520-0450\(2003\)042<0873:ACOVWP>2.0.CO;2](https://doi.org/10.1175/1520-0450(2003)042<0873:ACOVWP>2.0.CO;2).
- Schoeberl, M. R., A. R. Douglass, Z. Zhu, and S. Pawson, 2003: A comparison of the lower stratospheric age spectra derived from a general circulation model and two data assimilation systems. *J. Geophys. Res.*, **108**, 4113, <https://doi.org/10.1029/2002JD002652>.
- Sherwood, S. C., 2000: A stratospheric “drain” over the Maritime Continent. *Geophys. Res. Lett.*, **27**, 677–680, <https://doi.org/10.1029/1999GL010868>.
- Shibata, T., H. Vömel, S. Hamdi, S. Kaloka, F. Hasebe, M. Fujiwara, and M. Shiotani, 2007: Tropical cirrus clouds near cold point tropopause under ice supersaturated conditions observed by lidar and balloon-borne cryogenic frost point hygrometer. *J. Geophys. Res.*, **112**, D03210, <https://doi.org/10.1029/2006JD007361>.
- , and Coauthors, 2012: Cirrus cloud appearance in a volcanic aerosol layer around the tropical cold point tropopause over Biak, Indonesia, in January 2011. *J. Geophys. Res.*, **117**, D11209, <https://doi.org/10.1029/2011JD017029>.
- Shiotani, M., M. Fujiwara, F. Hasebe, H. Hashizume, H. Vömel, S. J. Oltmans, and T. Watanabe, 2002: Ozone-sonde observations in the equatorial eastern Pacific—The Shoyo-Maru survey. *J. Meteor. Soc. Japan*, **80**, 897–909, <https://doi.org/10.2151/jmsj.80.897>.
- Solomon, S., K. H. Rosenlof, R. W. Portmann, J. S. Daniel, S. M. Davis, T. J. Sanford, and G.-K. Plattner, 2010: Contributions of stratospheric water vapor to decadal changes in the rate of global warming. *Science*, **327**, 1219–1223, <https://doi.org/10.1126/science.1182488>.

- Stiller, G. P., and Coauthors, 2012: Observed temporal evolution of global mean age of stratospheric air for the 2002 to 2010 period. *Atmos. Chem. Phys.*, **12**, 3311–3331, <https://doi.org/10.5194/acp-12-3311-2012>.
- Sugawara, S., and Coauthors, 2018: Age and gravitational separation of the stratospheric air over Indonesia. *Atmos. Chem. Phys.*, **18**, 1819–1833, <https://doi.org/10.5194/acp-18-1819-2018>.
- Takashima, H., M. Shiotani, M. Fujiwara, N. Nishi, and F. Hasebe, 2008: Ozone sonde observations at Christmas Island (2°N, 157°W) in the equatorial central Pacific. *J. Geophys. Res.*, **113**, D10112, <https://doi.org/10.1029/2007JD009374>.
- Thompson, A. M., and Coauthors, 2003: Southern Hemisphere Additional Ozone sondes (SHADOZ) 1998–2000 tropical ozone climatology 1. Comparison with Total Ozone Mapping Spectrometer (TOMS) and ground-based measurements. *J. Geophys. Res.*, **108**, 8238, <https://doi.org/10.1029/2001JD000967>.
- Toyoda, S., N. Yoshida, T. Urabe, S. Aoki, T. Nakazawa, S. Sugawara, and H. Honda, 2001: Fractionation of N₂O isotopomers in the stratosphere. *J. Geophys. Res.*, **106**, 7515–7522, <https://doi.org/10.1029/2000JD900680>.
- , and Coauthors, 2018: Vertical distributions of N₂O isotopocules in the equatorial stratosphere. *Atmos. Chem. Phys.*, **18**, 833–844, <https://doi.org/10.5194/acp-18-833-2018>.
- Trismidianto, T. W. Hadi, S. Ishida, Q. Moteki, A. Manda, and S. Iizuka, 2016: Development processes of oceanic convective systems inducing the heavy rainfall over the western coast of Sumatra on 28 October 2007. *Sci. Online Lett. Atmos.*, **12**, 6–11, <https://doi.org/10.2151/sola.2016-002>.
- Tsuda, T., and Coauthors, 1995: A preliminary report on observations of equatorial atmosphere dynamics in Indonesia with radars and radiosondes. *J. Meteor. Soc. Japan*, **73**, 393–406, https://doi.org/10.2151/jmsj1965.73.2B_393.
- Vömel, H., D. E. David, and K. Smith, 2007: Accuracy of tropospheric and stratospheric water vapor measurements by the cryogenic frost point hygrometer: Instrumental details and observations. *J. Geophys. Res.*, **112**, D08305, <https://doi.org/10.1029/2006JD007224>.
- , T. Naebert, R. Dirksen, and M. Sommer, 2016: An update on the uncertainties of water vapor measurements using cryogenic frost point hygrometers. *Atmos. Meas. Tech.*, **9**, 3755–3768, <https://doi.org/10.5194/amt-9-3755-2016>.
- Waugh, D., 2009: The age of stratospheric air. *Nat. Geosci.*, **2**, 14–16, <https://doi.org/10.1038/ngeo397>.
- , and T. M. Hall, 2002: Age of stratospheric air: Theory, observations, and models. *Rev. Geophys.*, **40**, 1010, <https://doi.org/10.1029/2000RG000101>.
- WMO, 2014: Scientific assessment of ozone depletion. Global Ozone Research and Monitoring Project Rep. 55, WMO, 416 pp., www.esrl.noaa.gov/csd/assessments/ozone/2014/chapters/2014OzoneAssessment.pdf.